

Synthesis and characterization of tribenzyl ammonium-tribromide supported on magnetic Fe₃O₄ nanoparticles: a robust magnetically recoverable catalyst for the oxidative coupling of thiols and oxidation of sulfides

Lotfi Shiri¹ · Arash Ghorbani-Choghamarani¹ ·
Mosstafa Kazemi¹

Received: 30 July 2016 / Accepted: 19 October 2016 / Published online: 9 November 2016
© Springer Science+Business Media Dordrecht 2016

Abstract Taking into account the principles of green chemistry, magnetic nanoparticles, especially Fe₃O₄ nanoparticles, open up a new chapter in modern organic synthesis to inset a fascinating, stupendous and efficient catalytic strategy for facilitating catalyst recovery in various chemical reactions. Inspired by this topic, tribenzyl ammonium-tribromide immobilized on magnetic nanoparticles (Fe₃O₄–TBA–Br₃) as a bromine source was successfully synthesized and its catalytic activity in the oxidative coupling of thiols and oxidation of sulfides was investigated. It is the first report on the use of the immobilized bromine source on Fe₃O₄ nanoparticles as a nanomagnetic recyclable catalyst for the oxidative coupling of thiols. The nanosolid catalyst could be easily recovered by a simple magnetic separation and reused for several cycles without significant degradation in catalytic activity.

Electronic supplementary material The online version of this article (doi:[10.1007/s11164-016-2790-6](https://doi.org/10.1007/s11164-016-2790-6)) contains supplementary material, which is available to authorized users.

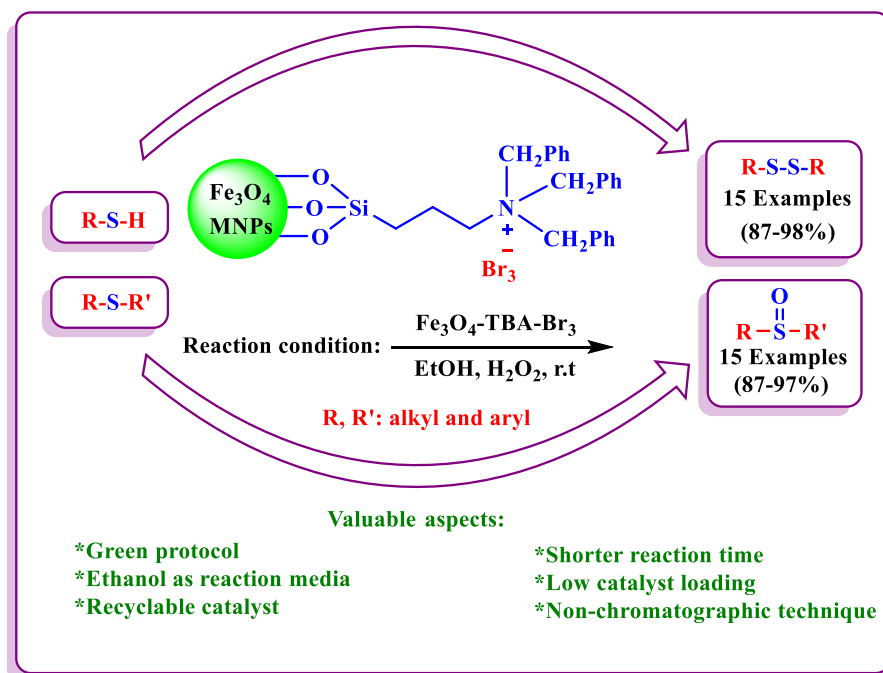
✉ Lotfi Shiri
Lshiri47@gmail.com

Arash Ghorbani-Choghamarani
Arashghch58@yahoo.com

Mosstafa Kazemi
Mosstafakazemi@gmail.com

¹ Department of Chemistry, Faculty of Basic Sciences, Ilam University, P.O. Box 69315-516, Ilam, Iran

Graphical Abstract



Keywords Bromine source · Oxidation · Thiols · Sulfides · External magnet · Recyclable catalyst

Introduction

Oxidative coupling of thiols and oxidation of sulfides are two fundamental transformations in organic chemistry because their products, namely disulfides and sulfoxides, respectively, are two important classes of organic sulfur compounds for which their application as precursors or intermediates in organic synthesis are highly regarded among organic chemists [1, 2]. Besides synthetic applications, interest in disulfides and sulfoxides has been amplified when it was revealed that they not only play a crucial role in the synthesis of natural products and valuable physiologically and pharmacologically active molecules but also exist as important integral and supplementary parts in many pharmaceutical and biological active molecules such as cystine, DTNB (Ellman's reagent or 5,50-dithio-bis(2-nitrobenzoic acid), omeprazole and fipronil [3–6]. These fascinating applications have recently stimulated organic chemists to apply more and more focus on new, clean and economic methodologies for the synthesis of disulfides and sulfoxides. During recent years, a diverse range of reagents, catalysts and oxidants have been reported for the performance of these transformations [7]. A series of tremendous properties such as being inexpensive and environmentally benign as well as producing water as

the only by-product has caused hydrogen peroxide to be more extensively employed in oxidation processes compared to other oxidants [8].

The easy recovery of catalysts and their reusability are two prominent characteristics in most of modern catalytic processes because either the employed catalysts are often very expensive or the targeted products are often very valuable from the economical and medicinal points of view [9, 10]. In this respect, as an important class of separable materials, magnetic nanoparticles (MNPs) have recently become a hot research topic in organic synthetic chemistry and material sciences, because of their high potential in catalysis and numerous applications in biomedicine [11]. Numerous recent studies reported in literature clearly demonstrated that among the various MNPs employed as the core magnetic support, Fe_3O_4 nanoparticles have received more special attention in modern catalysis research due to their tremendous properties such as simple synthesis and functionalization, abundance of unique activities, high stability, high surface area, low toxicity and price and simple separation by magnetic forces [12–14]. These attractive and valuable properties have caused Fe_3O_4 nanoparticles to emerge as a promising alternative to other catalyst supports [15].

Up to now, a diverse range of synthetic protocols have been developed for the construction of organic compounds and synthetic intermediates using molecular bromine [16]. To decrease the toxicity of molecular bromine (since molecular bromine is toxic), during the recent decades, a series of tribromide-containing compounds have been prepared and successfully applied as catalysts for organic reactions to obtain the corresponding targeted synthetic products [17, 18]. The immobilization of *N*-tribromide reagents on MNPs can be regarded as an efficient and fascinating catalytic strategy to overcome this drawback. Inspired by this catalytic strategy, we synthesized immobilized tribenzyl ammonium-tribromide on Fe_3O_4 nanoparticles ($\text{Fe}_3\text{O}_4\text{-TBA-Br}_3$) and studied their catalytic activities in the oxidative coupling of thiols and oxidation of sulfides. According to the best of our knowledge, it is the first report on the use of the immobilized bromine source on Fe_3O_4 nanoparticles as a nanomagnetic recyclable catalyst for the oxidative coupling of thiols.

Experimental

Materials

Chemicals were purchased from Fisher and Merck. The reagents and solvents used in this work were obtained from Sigma-Aldrich, Fluka or Merck and used without further purification. Nanostructures were characterized using a Holland Philips X-pert X-ray powder diffraction (XRD) diffractometer (Co $\text{K}\alpha$, radiation = 0.154056 nm), at a scanning speed of 2° min^{-1} from 10° to 100° . The particle size and morphology were investigated using a JEOL JEM-2010 scanning electron microscope at an accelerating voltage of 200 kV. The IR spectra of samples were recorded in KBr disks using a NICOLET Impact 410 spectrometer. The thermogravimetric analysis (TGA) curves are recorded using a PL-STA 1500 device

manufactured by Thermal Sciences. Supermagnetic properties of catalysts were measured on a VSM (MDKFD, Iran).

Preparation of the magnetic Fe₃O₄ nanoparticles

The mixture of FeCl₃·6H₂O (5.838 g, 0.0216 mol) and FeCl₂·4H₂O (2.147 g, 0.0108 mol) were dissolved in 100 mL of deionized water in a three-necked bottom (250 mL) under N₂ atmosphere. After that, under rapid mechanical stirring, 10 mL of NH₃ was added into the solution within 30 min with vigorous mechanical stirring. After being rapidly stirred for 30 min, the resultant black dispersion was heated to 80 °C for 30 min. The black precipitate formed was isolated by magnetic decantation, washed with double-distilled water until neutrality, and further washed twice with ethanol and dried at room temperature.

Preparation of Fe₃O₄-APTMS

The obtained Fe₃O₄ nanoparticles (1.5 g) were dispersed in 250 mL of ethanol/water (volume ratio, 1:1) by sonication for 30 min, and then APTMS (2.5 mL) was added to the mixture reaction. The reaction mixture was stirred using mechanical stirring under N₂ atmosphere at 40 °C for 8 h. Then, the nanoparticles were redispersed in ethanol by sonication for five times and separated through magnetic decantation. The nanoparticle product (Fe₃O₄-APTMS) was dried at room temperature.

Preparation of Fe₃O₄-TBA-Br

The obtained Fe₃O₄-APTMS (1 g) was added to a mixture of K₂CO₃ (2 mmol) and benzyl bromide (2.5 mL) in DMF. The mixture was then stirred at 80 °C for 30 h under N₂ atmosphere. The resulting powder was separated by magnetic decantation. The magnetic powder was washed with ethanol and dried at room temperature.

Preparation of Fe₃O₄-TBA-Br₃ catalyst

The Fe₃O₄-TBA-Br (1 g) was dispersed in CCl₄ (10 mL) by ultrasonic bath for 20 min. Subsequently, Br₂ (4 mL) was added and the mixture was stirred for 8 h at room temperature. Then, the final product was separated by magnetic decantation and washed by CCl₄ to remove the unattached substrates. The product (Fe₃O₄-TBA-Br₃) was stored in a refrigerator for use as a catalyst.

General procedure for the oxidative coupling of thiols to the disulfides

A mixture of thiol (1 mmol), hydrogen peroxide (0.5 mL) and the catalyst (0.005 g) in ethanol (2 mL) was stirred at ambient temperature. Reaction progress was monitored by TLC (acetone: *n*-hexane, 2:8). After completion of the reaction, catalyst was separated by an external magnet and washed with ethyl acetate; next, the product was extracted with ethyl acetate (5 mL × 4). The organic layer was

dried over anhydrous Na_2SO_4 (1.5 g). Finally, the organic solvents were evaporated, and the corresponding disulfides were obtained in high to excellent yields (88–98%).

General procedure for the oxidation of sulfides to the sulfoxides

The catalyst (0.010 g) was added to solution of sulfide (1 mmol) and H_2O_2 (0.5 mL) in ethanol (2 mL). The reaction mixture was stirred at room temperature, and the progress of the reaction was monitored by TLC (acetone:*n*-hexane, 2:8). After completion of the reaction, catalyst was separated by an external magnet and washed with ethyl acetate; next, the product was extracted with ethyl acetate (5 mL \times 4). The organic layer was dried over anhydrous Na_2SO_4 (1.5 g). Finally, the organic solvents were evaporated, and the corresponding sulfoxides were obtained in high to excellent yields (88–99%).

Spectroscopic data

All the products reported here are known compounds and the spectroscopic data was matched literature values. Data for the some of the compounds are given below.

1,2-Bis(4-methylphenyl)disulfane (2f)

^1H NMR (400 MHz, CDCl_3): δ = 2.62 (s, 6H), 6.88 (d, J = 8.8 Hz, 4H), 7.32 (d, J = 8.8 Hz, 4H) ppm. ^{13}C NMR (100 MHz, CDCl_3): δ = 22.1, 126.6, 128.8, 131.9, 135.5.

1,2-Bis(4-fluorophenyl)disulfane (2g)

^1H NMR (400 MHz, CDCl_3): δ = 7.47 (d, J = 8.8 Hz, 4H), 7.56 (d, J = 8.8 Hz, 4H) ppm. ^{13}C NMR (100 MHz, CDCl_3): δ = 119.46, 129.48, 132.27, 145.32.

1,2-Bis(4-bromophenyl)disulfane (2h)

^1H NMR (400 MHz, CDCl_3): δ = 7.54 (d, J = 8.8 Hz, 4H), 8.23 (d, J = 8.8 Hz, 4H) ppm. ^{13}C NMR (100 MHz, CDCl_3): δ = 115, 121.3, 131.9, 139.1.

1,2-Dibenzylsulfane (2m)

^1H NMR (400 MHz, CDCl_3): δ = 3.75 (s, 4H), 7.03–7.15 (m, 10H) ppm. ^{13}C NMR (100 MHz, CDCl_3): δ = 43.35, 128.34, 128.51, 129.13, 137.49.

Methyl phenyl sulfoxide (4a)

^1H NMR (400 MHz, CDCl_3): δ = 2.68 (s, 3 H, CH_3), 7.45–7.62 (m, 5 H, ArH). ^{13}C NMR (100 MHz, CDCl_3): δ 43.92, 123.47, 129.35, 131.05, 145.60.

Benzyl phenyl sulfoxide (4b)

^1H NMR (400 MHz, CDCl_3): δ = 4.02 (d, 1 H, J = 12.8 Hz), 4.11 (d, 1 H, J = 12.8 Hz), 6.99–7.01 (d, 2 H), 7.25–7.50 (m, 8 H). ^{13}C NMR (100 MHz, CDCl_3): δ 63.57, 124.45, 128.27, 128.47, 128.88, 129.13, 130.39, 131.20, 142.74.

Benzyl 4-methylphenyl sulfoxide (4e)

^1H NMR (400 MHz, CDCl_3): δ = 2.43 (s, 3 H), 4.00 (d, 2 H, J = 12.8 Hz), 4.12 (d, 2 H, J = 12.4 Hz), 7.02–7.31 (m, 9 H). ^{13}C NMR (100 MHz, CDCl_3): δ 21.49, 63.70, 124.50, 128.21, 128.48, 129.33, 129.59, 130.40, 130.52, 141.67.

4-Chlorobenzyl 4-methylphenyl sulfoxide (4f)

^1H NMR (400 MHz, CDCl_3): δ = 2.43 (s, 3 H), 4.00 (s, 2 H), 6.92–6.94 (d, 2 H, J = 8 Hz), 7.23–7.30 (m, 6 H). ^{13}C NMR (100 MHz, CDCl_3): δ 21.49, 62.52, 124.42, 127.66, 128.59, 129.78, 131.69, 134.34, 139.19, 141.84.

Benzyl 4-bromophenyl sulfoxide (4g)

^1H NMR (400 MHz, CDCl_3): δ = 4.02 (d, 2 H, J = 12 Hz), 4.13 (d, 2 H, J = 12 Hz), 6.99–7.59 (m, 9 H). ^{13}C NMR (100 MHz, CDCl_3): δ 63.42, 125.66, 126.07, 128.48, 128.60, 130.40, 132.05, 141.83.

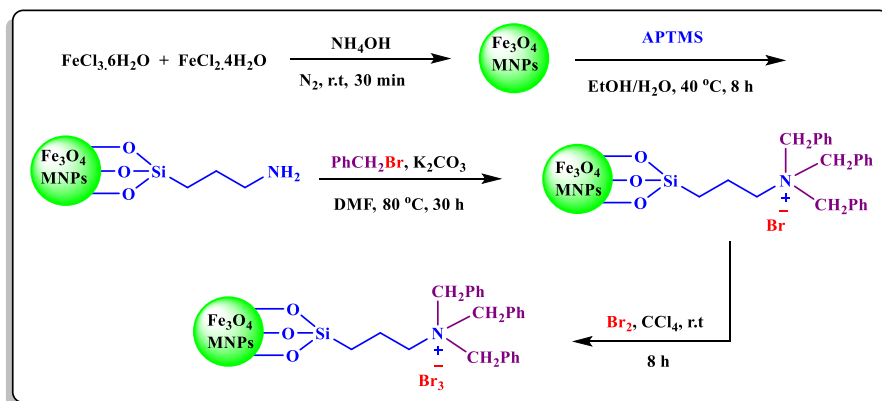
Dibenzyl sulfoxide (4j)

^1H NMR (400 MHz, CDCl_3): δ = 3.898 (d, 2 H, J = 12.8 Hz), 3.957 (d, 2 H, J = 12.8 Hz), 7.29–7.43 (m, 10 H). ^{13}C NMR (100 MHz, CDCl_3): δ 57.28, 128.40, 128.99, 130.15, 130.18.

Results and discussion

Preparation and characterization of Fe_3O_4 -TBA- Br_3

Immobilized tribenzyl ammonium-tribromide on Fe_3O_4 nanoparticles (Fe_3O_4 -TBA- Br_3 catalyst) was successfully synthesized by using the surface modification strategy as depicted in Scheme 1. The Fe_3O_4 nanoparticles were prepared by a chemical coprecipitation method [19] and coated with 3-aminopropyltrimethoxysilane (APTMS) by covalent bonds [19]. The immobilized ammonium bromide on Fe_3O_4 nanoparticles (Fe_3O_4 -TBA-Br) was prepared through the reaction of the supported APTMS with tribenzyl bromide in the presence of K_2CO_3 in DMF (dimethylformamide) under reflux conditions for 30 h. Finally, the reaction of Fe_3O_4 -TBA-Br with Br_2 in tetrachloride carbon at ambient temperature for 8 h led to generation of immobilized tribenzyl ammonium-tribromide on Fe_3O_4 nanoparticles (Fe_3O_4 -TBA- Br_3).



Scheme 1 General route for the synthesis of $\text{Fe}_3\text{O}_4\text{-TBA-Br}_3$

The synthesized nanomagnetic catalyst was comprehensively characterized by Fourier transform infrared (FT-IR) spectroscopy, thermogravimetric analysis (TGA), X-ray diffraction (XRD), scanning electron microscopy (SEM), X-ray spectroscopy (EDX) and vibrating sample magnetometer (VSM) analysis techniques.

The successful immobilization of tribenzyl ammonium-tribromide on Fe_3O_4 nanoparticles ($\text{Fe}_3\text{O}_4\text{-TBA-Br}_3$ catalyst) was confirmed by the FT-IR spectra. The FT-IR spectra for the Fe_3O_4 MNPs (a), $\text{Fe}_3\text{O}_4\text{-APTMS}$ (b), $\text{Fe}_3\text{O}_4\text{-TBA-Br}$ (c) and $\text{Fe}_3\text{O}_4\text{-TBA-Br}_3$ are shown in Fig. 1. As seen on Fig. 1, the FT-IR analysis of Fe_3O_4 MNPs (a) shows a strong peak at 579 cm^{-1} , which is attributed to the presence of an Fe–O bond and it guarantees the formation of Fe_3O_4 MNPs. In the curve of Fe_3O_4 MNPs (a), a broad peak is observed at 3401 cm^{-1} , which it is the characteristic of both symmetrical and unsymmetrical modes of O–H bonds linked to the surface iron atoms. Also, the existence of a stretch peak at 1625 cm^{-1} is attributed to an adsorbed water layer. The presence of the APTMS moiety on the surface of the Fe_3O_4 MNPs is confirmed by a characteristic peak at 1002 cm^{-1} which is ascribed to the Fe–O–Si stretching vibration. The FT-IR analysis of the $\text{Fe}_3\text{O}_4\text{-APTMS}$ (b) exhibits a broad bond at 3434 cm^{-1} that is assigned to an NH_2 group, and two weak peaks at 2922 and 2854 cm^{-1} are ascribed to the C–H stretching vibration of the alkyl chain of amine. In the curve of $\text{Fe}_3\text{O}_4\text{-TBA-Br}$ (c), the characteristic weak peaks at 2926 and 1642 cm^{-1} are attributed to C–H and C=C stretching vibration. Also, the broad peak at nearly $1370\text{--}1400 \text{ cm}^{-1}$ in the $\text{Fe}_3\text{O}_4\text{-TBA-Br}$ (c) is attributed to C–N⁺ stretching vibration [20]. But, Br_3 exhibits a signal between 180 and 200 cm^{-1} [20], which is not recognizable with the FT-IR spectrum.

The morphology and size of the $\text{Fe}_3\text{O}_4\text{-TBA-Br}_3$ catalyst was investigated by SEM as shown in Fig. 2. From SEM images, it can be seen that the catalyst was made up uniformly and the average size of $\text{Fe}_3\text{O}_4\text{-TBA-Br}_3$ is about 10 nm.

The components of $\text{Fe}_3\text{O}_4\text{-TBA-Br}_3$ were analyzed by using energy-dispersive EDX (Fig. 3). As shown in Fig. 3, the characteristic peaks of Fe, O, C, N, Si and Br showed well that the tribenzyl ammonium-tribromide was successfully immobilized

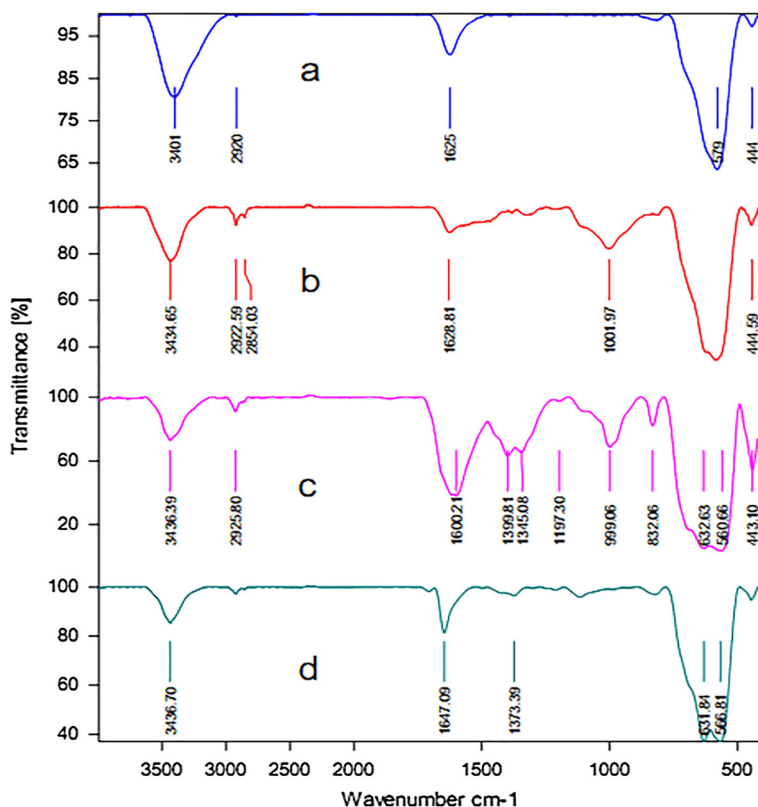


Fig. 1 FT-IR spectra of Fe₃O₄ MNPs (a) Fe₃O₄-APTMS (b), Fe₃O₄-TBA-Br (c) and Fe₃O₄-TBA-Br₃. (Color figure online)

on Fe₃O₄ nanoparticles. As a result of this analysis, it can be concluded that the Fe₃O₄-TBA-Br₃ nanomagnetic catalyst has been successfully synthesized.

The magnetic property of the catalyst was investigated by VSM at ambient temperature. The curves of magnetization for the Fe₃O₄ nanoparticles (red line) and Fe₃O₄-TBA-Br₃ (green line) are depicted in Fig. 4. As shown on Fig. 4, the saturation magnetization of Fe₃O₄-TBA-Br₃ was found to be at about 38 emu g⁻¹, which is much lower than bare Fe₃O₄ MNPs (about 55 emu g⁻¹). The decrease of the saturation magnetization can be related to the presence of tribromide groups on the surface of the Fe₃O₄ nanoparticles supports.

TGA is an effective and fascinating spectra technique to investigate the thermal stability of the immobilized catalyst relative to that of MNPs. Furthermore, the bond formation between the MNPs and the catalyst can be as well interpreted and verified by TGA. The overlaid TGA curves of Fe₃O₄ nanoparticles (green line), Fe₃O₄-APTMS (red line) and Fe₃O₄-TBA-Br₃ (blue line) are displayed in Fig. 5. The initial mass loss at temperatures at below 200 °C is due to the removal of physically adsorbed solvent and surface hydroxyl groups. Organic groups have been reported to desorb at temperatures above 260 °C. The mass percentage loss of about 3.5%

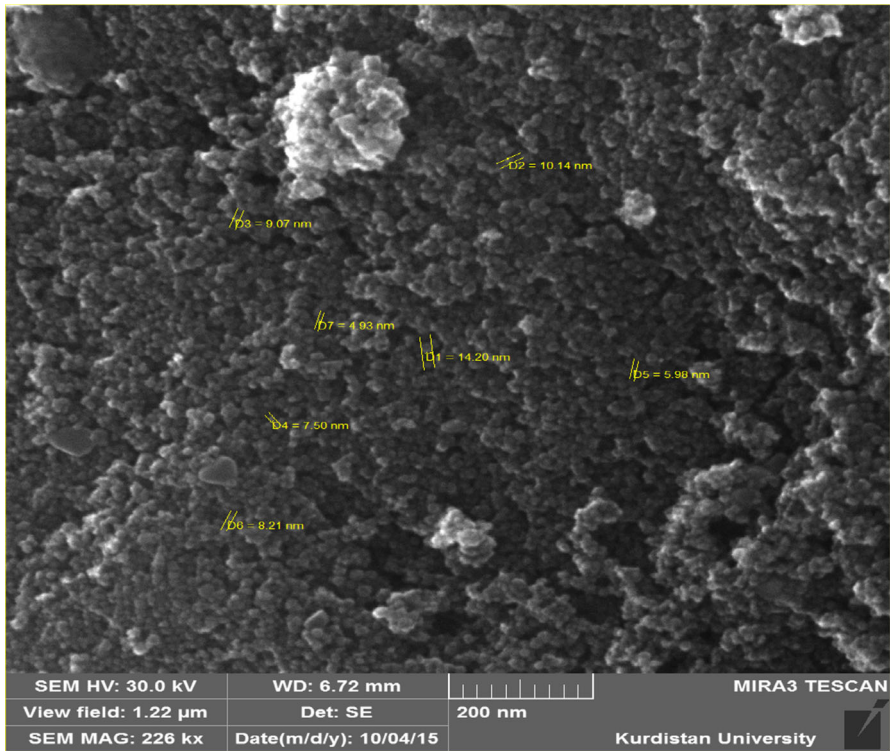


Fig. 2 SEM image of the Fe₃O₄-TBA-Br₃

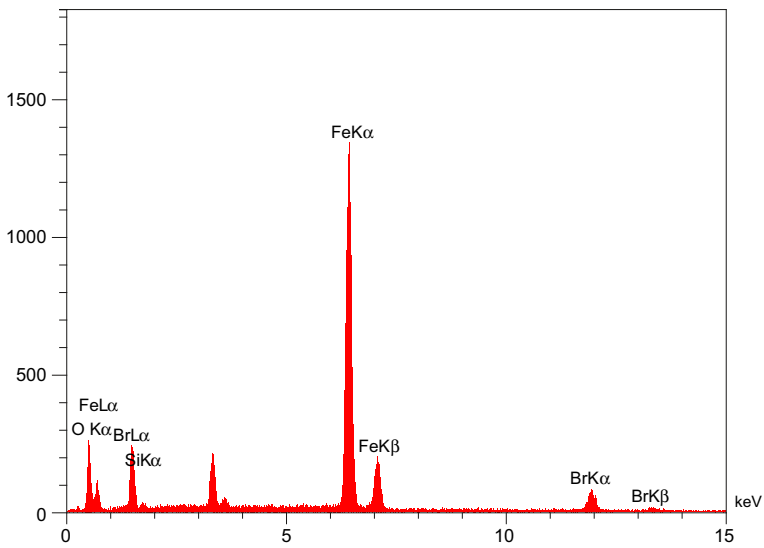


Fig. 3 EDX spectrum of the Fe₃O₄-TBA-Br₃

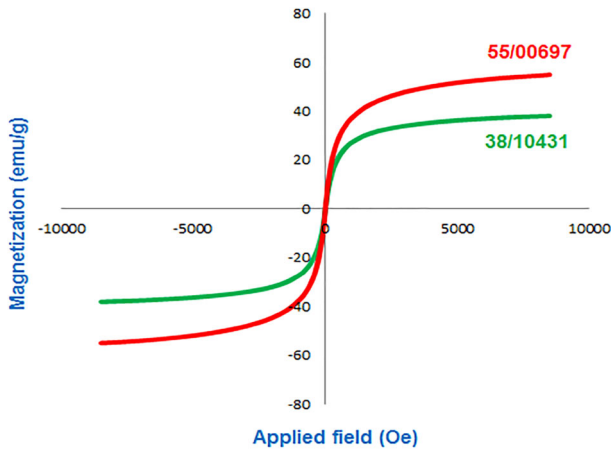


Fig. 4 Magnetization curves for Fe₃O₄ MNPs (red line) and Fe₃O₄-TBA-Br₃ (green line) at room temperature. (Color figure online)

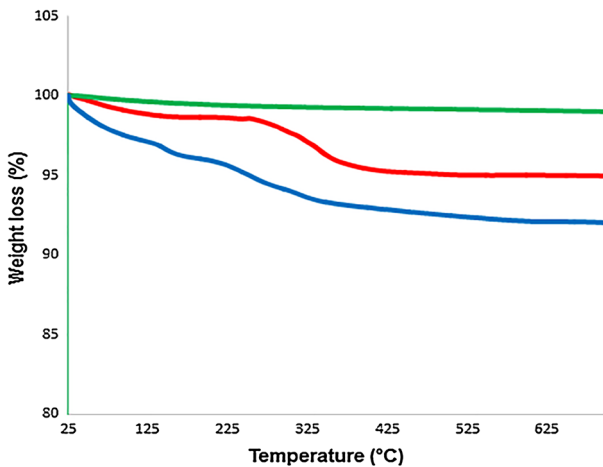


Fig. 5 TGA curves of Fe₃O₄ MNPs (green line), Fe₃O₄-APTMS (red line) and Fe₃O₄-TBA-Br₃ (blue line). (Color figure online)

between 250 and 475 °C for Fe₃O₄-APTMS is ascribed to the thermal decomposition of the 3-aminopropyl silane groups. In the curve of Fe₃O₄-TBA-Br₃, a weight percentage loss about 4% over the range of 200–620 °C is also observed, which is attributed to the breakdown of the tribenzyl ammonium-tribromide moieties. As the result of this analysis, it can be concluded that the effective grafting of tribenzyl ammonium-tribromide groups (TBA-Br₃) on the Fe₃O₄ nanoparticles is verified.

XRD is an effective spectra analysis technique to achieve better reorganization of the major properties of the magnetite structures. In fact, the formation of a magnetite crystal phase in the nanomagnetic catalyst in aggregate powder form can also be identified by the XRD. The XRD patterns of the prepared Fe₃O₄ MNPs (blue

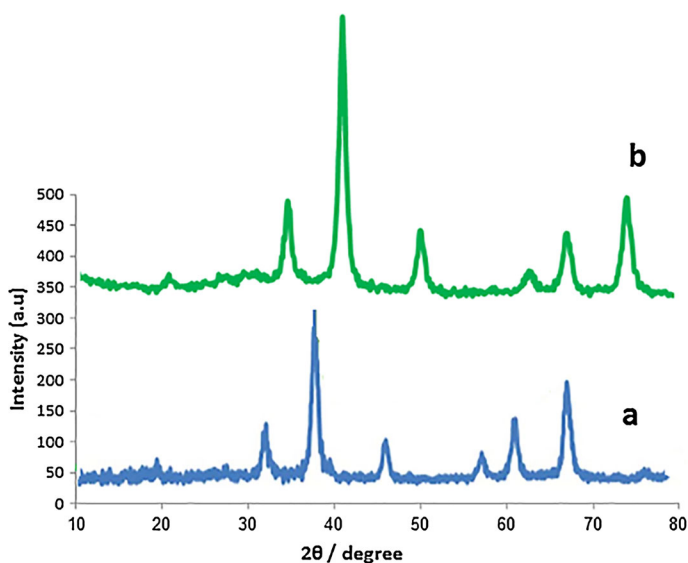
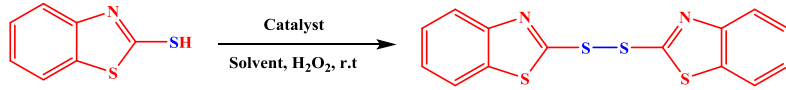


Fig. 6 The XRD patterns of Fe₃O₄ MNPs (*a*) and Fe₃O₄-TBA-Br₃ (*b*)

line or **a**) and Fe₃O₄-TBA-Br₃ (green line or **b**) are presented in Fig. 6. In the XRD pattern of Fe₃O₄-TBA-Br₃, six characteristic peaks at $2\theta = 35.1^\circ$, 41.4° , 50.6° , 63.2° , 67.5° and 74.5° were observed, which are assigned to the (220), (311), (400), (422), (511) and (440) crystallographic faces of magnetite (in good agreement with the standard Fe₃O₄ XRD spectrum reported in literature) [14]. This analysis clearly affirmed the theme that the surface modification and conjugation of the Fe₃O₄ nanoparticles did not lead to a phase change.

Catalytic studies

After characterization of the catalyst, the catalytic activity of Fe₃O₄-TBA-Br₃ in the oxidative coupling of thiols to the disulfides and also oxidation sulfides to the sulfoxides at ambient temperature was studied. To find out the optimum reaction conditions and understand the effects of various parameters (such as solvent type, catalyst and hydrogen peroxide amounts) on these oxidation processes, the room temperature oxidative coupling of benzo[d]thiazole-2-thiol was chosen as a model substrate (Table 1). In the preliminary stage of this investigation, the room temperature oxidative coupling of benzo[d]thiazole-2-thiol using H₂O₂ (0.5 mL) in EtOH was performed using different amounts of catalyst. As shown in Table 1, at a lower catalyst amount (3 mg), a 92% yield of benzo[d]thiazole-2-thiol was observed after 20 min (Table 1, entry 1). On increasing the catalyst weight to 5 mg, the yield of benzo[d]thiazole-2-thiol increased up to 95% after 10 min (Table 1, entry 2). The increase in the product yield with an increase in the catalyst weight can be attributed to an increase in the availability of catalytically active sites required for this oxidation reaction. On further increasing the amount of catalyst, namely, amounts

Table 1 Optimization of the reaction conditions


Entry	Catalyst (mg)	H ₂ O ₂ (mL)	Solvent (temp. °C)	2d	
				Time/min	Yield (%) ^a
1	3	0.5	EtOH (r.t)	20	92
2	5	0.5	EtOH (r.t)	10	98*
3	10	0.5	EtOH (r.t)	10	97
4	15	0.5	EtOH (r.t)	10	98
5	–	0.5	EtOH (r.t)	120	5
6	5	0.5	CH ₃ CN (r.t)	20	96
7	5	0.5	Acetone (r.t)	25	95
8	5	0.5	THF (r.t)	100	93
9	5	0.5	CH ₂ Cl ₂ (r.t)	85	93
10	5	0.5	H ₂ O (r.t)	60	30 ^b
11	5	0.3	EtOH (r.t)	55	91
12	5	0.4	EtOH (r.t)	30	95
13	5	0.6	EtOH (r.t)	10	98
14	5	0.5	EtOH (40 °C)	10	97

* and bold value indicate the optimal conditions

Reaction conditions: the oxidative coupling of benzo[d]thiazole-2-thiol (1 mmol) using 30% H₂O₂ in the presence of catalyst and solvent (2 mL)

^a Isolated yield

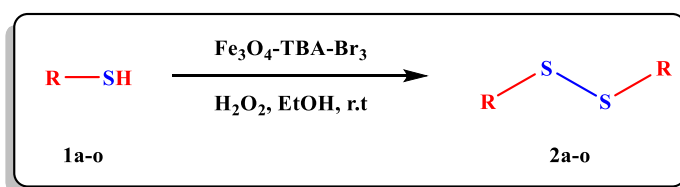
^b Substrate was insoluble in water

greater than 5 mg, any appreciable change or improvement wasn't observed in product yield after 10 min (Table 1, entries 3–4). The collected results in Table 1 clearly demonstrate that the reaction rate and product yield not only depended strongly on the amount of the catalyst (Table 1, entries 1–4), but also that the presence of catalyst is a vital topic in this process because it was found that once the reaction was carried out in the absence of a nanomagnetic catalyst, only 5% yield of the desired product was observed after 120 min (using column chromatography; Table 1, entry 5). Next, using an optimal catalytic amount of Fe₃O₄-TBA-Br₃ (5 mg), the room temperature oxidative coupling of benzo[d]thiazole-2-thiol in several prevalent solvents was carried out to assess the role of solvent on the process (Table 1, entries 6–10). Among the various solvents, such as EtOH, CH₃CN, acetone, CH₂Cl₂, THF and water it, was found that EtOH was the most effective solvent and gave the highest yield of the desired product within a short period of time, namely, less than 10 min (Table 1, entry 2). After selecting the ideal solvent, using an optimal catalytic amount of Fe₃O₄-TBA-Br₃ (5 mg), the room temperature oxidative coupling of benzo[d]thiazole-2-thiol in EtOH was also studied with varied amounts of 30% H₂O₂, and the results are represented in Table 1 (entries 11–13).

Finally, using the optimal catalyst and H_2O_2 amount, the model reaction in EtOH at 40 °C was tested, but, any appreciable change or improvement wasn't observed in product yield after 10 min. From Table 1 it is found that 0.5 mL of hydrogen peroxide exhibits the best performance for the present process. Therefore, the highest yield and shortest reaction time of product **2d** was obtained in the presence of 5 mg $\text{Fe}_3\text{O}_4\text{-TBA-Br}_3$ and 0.5 mL of 30% hydrogen peroxide in EtOH (2 mL) at ambient temperature (Table 1, entry 2).

With the optimized reaction conditions in hand, to further understand the scope and generality of this catalytic system, the applicability of various thiols were next subjected to the oxidation reaction (Scheme 2). The results of this study are listed in Table 2. It is noteworthy that in all of the oxidative couplings, no product was observed and the desired products were obtained in short times and in high to excellent yields. As shown in Table 2, a diverse range of thiols including aromatic thiols (Table 2, entries 1–2) and heteroaromatic thiols (Table 2, entries 3–5), benzylic thiol (Table 2, entry 13) and aliphatic thiols (Table 2, entries 14–15) were successfully transformed into the corresponding disulfides. The obtained results demonstrated well that the reaction rate, selectivity and product yield of the oxidative reactions depend on the type of thiol moieties because aromatic thiols were oxidized to the corresponding disulfides in shorter times and higher yields than aliphatic thiols. Also, aromatic and heteroaromatic thiols with electron-donating as well as electron-withdrawing substituents at ortho and para positions were well-tolerated and did not exert any tangible effect on the yield of reactions (Table 2, entries 6–12).

The tremendous and fascinating results obtained in the oxidative coupling of thiols encouraged us to apply more and more focus on $\text{Fe}_3\text{O}_4\text{-TBA-Br}_3$ and its catalytic activity in other organic transformations. In this respect, to find out the general applicability and efficiency of the catalyst, the catalytic activity of $\text{Fe}_3\text{O}_4\text{-TBA-Br}_3$ in the oxidation of sulfides to sulfoxides was also studied. Therefore, methyl phenyl sulfide (**4a**) was selected as a model substrate and it was observed that under the optimized reaction conditions for the oxidative coupling of thiols, the methyl phenyl sulfide oxidized smoothly to corresponding sulfoxide as the only product [as per thin layer chromatography (TLC)], and it is noteworthy that sulfone as an over-oxidation product isn't formed under these conditions. After ensuring the transformation, to understand the optimum reaction conditions, the impact of various parameters (such as solvent type, catalyst and hydrogen peroxide amounts) on the process (methyl phenyl sulfide as a model substrate) was studied. The best results (with respect to product yield and reaction time) for product **4a** were



Scheme 2 $\text{Fe}_3\text{O}_4\text{-TBA-Br}_3$ catalyzed the oxidative coupling of thiols to the disulfides

Table 2 Fe₃O₄-TBA-Br₃ catalyzed the oxidative coupling of thiols to the disulfides in ethanol at room temperature

Entry	Thiol	Product	Time (min)	Yield (%) ^a	Mp (°C) [References]
1	Benzenethiol	2a	40	91	59–61 [21]
2	Naphthalene-2-thiol	2b	15	92	134–135 [4]
3	Pyridine-2-thiol	2c	45	90	56–57 [22]
4	Benzo[d]thiazole-2-thiol	2d	10	98	172–173 [4]
5	Benzo[d]oxazole-2-thiol	2e	35	87	93–95 [4]
6	4-Methylbenzenethiol	2f	10	98	39–41 [4]
7	4-Fluorobenzenethiol	2g	15	92	Oil [23]
8	4-Bromobenzenethiol	2h	20	97	89–90 [22]
9	2-Aminobenzenethiol	2i	25	93	81–83 [24]
10	2-Mercaptobenzoic acid	2j	20	95	284–287 [5]
11	2,6-Dichlorobenzenethiol	2k	45	92	88–90 [22]
12	4,6-Dimethylpyrimidine-2-thiol	2l	35	91	160–162 [24]
13	Phenylmethanethiol	2m	45	94	69–70 [5]
14	2-Mercaptoethanol	2n	40	92	Oil [5]
15	2-Mercaptoacetic acid	2o	35	90	Oil [5]

^a Isolated yield

observed when the process was carried out in the presence of 10 mg of Fe₃O₄-TBA-Br₃ and 0.5 mL of 30% hydrogen peroxide in EtOH (2 mL) at ambient temperature. Accordingly, a number of aliphatic and aromatic sulfides were subjected to oxidation under the optimized reaction conditions (Scheme 3) and the results of this study are summarized in Table 3. It is noteworthy that all corresponding sulfoxides were obtained in excellent yields within a relatively short period of time. The presented results in Table 3 show well that aromatic sulfides are found to be more reactive and provided better product yields than aliphatic sulfides.

The high potential of this catalyst is shown by comparison of our results on the oxidative coupling of 4-methylbenzenethiol and oxidation of methyl phenyl sulfide with the previously reported protocols in the literature (Table 4). As

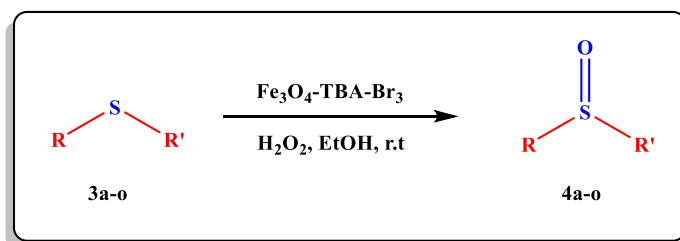
**Scheme 3** Fe₃O₄-TBA-Br₃ catalyzed the oxidative coupling of thiols to the disulfides

Table 3 $\text{Fe}_3\text{O}_4\text{-TBA-Br}_3$ catalyzed the oxidation of sulfides into sulfoxides in ethanol at room temperature

Entry	Sulfide	Product	Time (min)	Yield (%) ^a	Mp (°C) [References]
1	Methyl phenyl sulfide	4a	25	97	Oil [5]
2	Benzyl phenyl sulfide	4b	40	95	115–117 [4]
3	Ethyl phenyl sulfide	4c	60	94	Oil [24]
4	Methyl furfuryl sulfide	4d	10	93	Oil [5]
5	Benzyl 4-methylphenyl sulfide	4e	35	92	120–121 [25]
6	4-Chlorobenzyl 4-methylphenyl sulfide	4f	50	87	157–159 [25]
7	Benzyl 4-bromophenyl sulfide	4g	45	90	141–142 [25]
8	2-(Methylthio)ethanol	4h	10	88	Oil [24]
9	2-(Phenylthio)ethanol	4i	10	87	Oil [5]
10	Dibenzyl sulfide	4j	55	91	137–138 [4]
11	Dodecyl sulfide	4k	280	89	87–89 [4]
12	Dibutyl sulfide	4l	15	92	Oil [5]
13	Dipropyl sulfide	4m	40	94	Oil [5]
14	Diethyl sulfide	4n	65	90	Oil [5]
15	Tetrahydrothiophene	4o	10	93	Oil [5]

^a Isolated yield**Table 4** Comparison of $\text{Fe}_3\text{O}_4\text{-TBA-Br}_3$ for the oxidative coupling of 4-methylbenzenethiol and oxidation of methyl phenyl sulfide with previously reported catalysts

Entry	Substrate	Catalyst	Time (min)	Yield (%) ^a	References
1	4-Methylbenzenethiol	Ni-salen-MCM-41	25	95	[6]
2	4-Methylbenzenethiol	Fe NPs@SBA-15	45	94	[26]
3	4-Methylbenzenethiol	Zr-oxide@MCM-41	30	98	[5]
4	4-Methylbenzenethiol	Cu(II) Schiff base MCM-41	72	83	[22]
5	4-Methylbenzenethiol	Mn-ZSM-5	360	82	[27]
6	4-Methylbenzenethiol	$\text{Fe}_3\text{O}_4\text{-TBA-Br}_3$	10	98	This work
7	Methyl phenyl sulfide	NBS	270	93	[28]
8	Methyl phenyl sulfide	TsOH	240	88	[29]
9	Methyl phenyl sulfide	Ni-salen-MCM-41	156	95	[6]
10	Methyl phenyl sulfide	Zr-oxide@MCM-41	300	98	[5]
11	Methyl phenyl sulfide	Cu(II) Schiff base MCM-41	20	93	[22]
12	Methyl phenyl sulfide	$\text{Fe}_3\text{O}_4\text{-TBA-Br}_3$	25	97	This work

^a Isolated yield

shown in Table 4, the previously reported methods suffer from one or more drawbacks such as longer reaction time, using transition metal catalysts and low yields of products.

Reusability of the $\text{Fe}_3\text{O}_4\text{-TBA-Br}_3$ catalyst

The recovery and reusability of catalyst is a valuable advantage in modern catalysis research, which makes catalysts very notable from commercial and economical points of view. In this respect, the recyclability of $\text{Fe}_3\text{O}_4\text{-TBA-Br}_3$ was investigated in the oxidative coupling of 4-methylbenzenethiol and oxidation of methyl phenyl sulfide. At the end of the process, the $\text{Fe}_3\text{O}_4\text{-TBA-Br}_3$ was readily separated from the reaction mixture by an external magnet, washed several times with ethyl acetate and dried to remove residual product. Then, the recovered catalyst was reused for a subsequent fresh batch of the reaction. The catalytic activity was studied for five successive times and it showed similar activity (Fig. 7). Accordingly, one of the fascinating advantages of this new catalytic system is the simple, rapid and efficient separation of the catalyst by using a suitable external magnet, which minimizes the loss of catalyst during separation.

Also, the SEM image of the recovered catalyst is shown in Fig. 8. From the comparison of Figs. 8 with 2, it can be concluded that there aren't any significance differences in the morphologies of freshly prepared catalysts and the recovered catalyst after operation for five consecutive reaction cycles.

Conclusion

In this research, the tribenzyl ammonium-tribromide supported onto magnetic Fe_3O_4 nanoparticles ($\text{Fe}_3\text{O}_4\text{-TBA-Br}_3$) was introduced as a novel, stable, versatile and recyclable nanomagnetic catalyst for the oxidative coupling of thiols and oxidation of sulfides. The synthesized catalyst exhibits excellent activity in the synthesis of disulfides and sulfoxides in an economical and eco-friendly strategy. The $\text{Fe}_3\text{O}_4\text{-TBA-Br}_3$ catalyst with high activity could be readily recovered from reaction media by an external magnet and reused at least five successive times

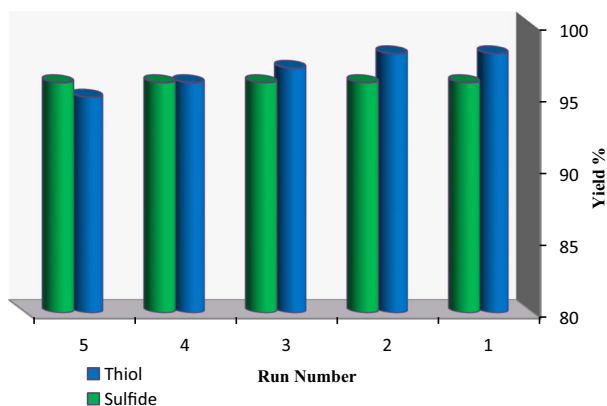


Fig. 7 Reusability of $\text{Fe}_3\text{O}_4\text{-TBA-Br}_3$ in the oxidative coupling of 4-methylbenzenethiol and oxidation of methyl phenyl sulfide

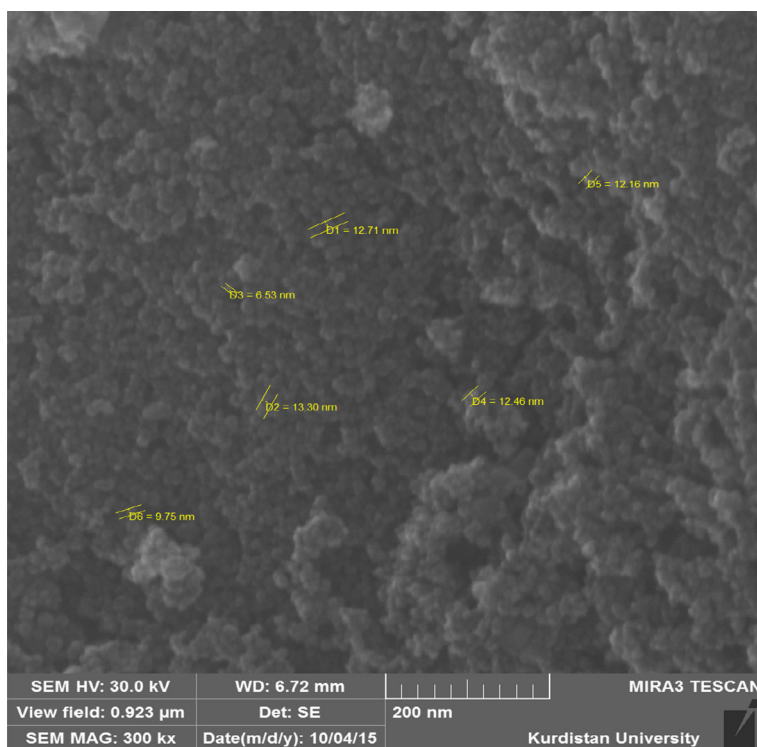


Fig. 8 SEM image of the recovered catalyst ($\text{Fe}_3\text{O}_4\text{-TBA-Br}_3$) after five cycles

without any noticeable loss of activity. According to the best of our knowledge, this is the first report on the use of the immobilized bromine source on magnetic Fe_3O_4 nanoparticles as a nanomagnetic recyclable catalyst for the oxidative coupling of thiols. The high to excellent yields of products, simplicity operation, use of ethanol as a solvent, easy magnetic separation and reusability as well as high activity of the catalyst are notable advantages of this strategy. As a result of this study, we believe that this catalytic system will open up a new avenue to introduce new, versatile and efficient bromine sources (as reusable nanomagnetic catalysts) for the synthesis of biologically and pharmaceutically active molecules.

Acknowledgements This work was supported by the research facilities of Ilam University, Ilam, Iran.

References

1. L. Teuber, *Sulfur Rep.* **31**, 257–349 (1992)
2. S.J. Behroozi, W. Kim, K.S. Gates, *J. Org. Chem.* **60**, 3964–3966 (1995)
3. M. Kazemi, L. Shiri, *J. Sulfur Chem.* **36**, 613–623 (2015)
4. A. Ghorbani-Choghamarani, B. Ghasemi, Z. Safari, G. Azadi, *Catal. Commun.* **60**, 70–75 (2015)
5. M. Hajjami, L. Shiri, A. Jahanbakhshi, *Appl. Organomet. Chem.* **29**, 668–673 (2015)
6. M. Nikoorazm, A. Ghorbani-Choghamarani, H. Mahdavi, S.M. Esmaceli, *Microporous Microporous Mater.* **211**, 174–178 (2015)

7. A. Ghorbani-Choghamarani, Z. Darvishnejad, B. Tahmasbi, *Inorg. Chim. Acta* **435**, 223–231 (2015)
8. S. Bonollo, D. Lanari, L. Vaccaro, *Eur. J. Org. Chem.* **14**, 2587–2598 (2011)
9. M. Kazemi, L. Shiri, H. Kohzadi, *Phosphorus Sulfur Silicon Relat. Elem.* **190**, 978–1003 (2015)
10. M. Sheykhani, L. Mamani, A. Ebrahimi, A. Heydari, *J. Mol. Catal. A: Chem.* **335**, 253–261 (2011)
11. B. Panella, A. Vargas, A. Baiker, *J. Catal.* **261**, 88–93 (2009)
12. L. Shiri, A. Ghorbani-Choghamarani, M. Kazemi, *Aust. J. Chem.* **69**, 585–600 (2016)
13. L. Shiri, A. Ghorbani-Choghamarani, M. Kazemi, *Aust. J. Chem.* (2016). doi:10.1071/CH16318 (in press)
14. A. Ghorbani-Choghamarani, M. Norouzi, *J. Mol. Catal. A Chem.* **395**, 172–179 (2014)
15. A. Ghorbani-Choghamarani, G. Azadi, *RSC Adv.* **5**, 9752–9758 (2015)
16. A. Ghorbani-Choghamarani, H. Goudarziafshar, P. Zamani, *Chin. Chem. Lett.* **22**, 1207–1210 (2011)
17. A.T. Khan, M. Lal, M.M. Khan, *Tetrahedron Lett.* **51**, 4419–4424 (2010)
18. A. Ghosh, A.T. Khan, *Tetrahedron Lett.* **55**, 2006–2009 (2014)
19. A. Rostami, B. Tahmasbi, H. Gholami, H. Taymorian, *Chin. Chem. Lett.* **24**, 211–214 (2013)
20. F.M. Moghaddam, N. Masoud, B.K. Foroushani, S. Saryazdi, N. Ghonouei, E. Daemi, *Sci. Iran.* **20**, 598–602 (2013)
21. T. Tabari, H. Tavakkoli, *Chin. J. Catal.* **33**, 1791–1796 (2012)
22. M. Nikoorazm, A. Ghorbani-Choghamarani, N. Noori, *J. Porous Mater.* **22**, 877–885 (2015)
23. A. Ghorbani-Choghamarani, M. Nikoorazm, H. Goudarziafshar, M. Abbasi, *Bull. Korean Chem. Soc.* **32**, 693–696 (2011)
24. A. Ghorbani-Choghamarani, B. Tahmasbi, F. Arghand, S. Faryadi, *RSC Adv.* **5**, 92174–92183 (2015)
25. M.M. Khodaeia, K. Bahramia, M.S. Arabi, *J. Sulfur Chem.* **31**, 83–88 (2010)
26. F. Rajabi, T. Kakeshpour, M.R. Saidi, *Catal. Commun.* **40**, 13–17 (2013)
27. A.K. Patra, A. Dutta, M. Pramanik, M. Nandi, H. Uyama, A. Bhaumik, *Chem. Catal. Chem.* **6**, 220–229 (2014)
28. B. Karimi, D. Zareyee, *J. Iran. Chem. Soc.* **5**, 5103–5107 (2008)
29. B. Yu, C.X. Guo, C.L. Zhong, Z.F. Diao, L.N. He, *Tetrahedron Lett.* **55**, 1818–1821 (2015)